

Keeping global warming within 1.5°C constrains emergence of aridification

Chang-Eui Park¹, Su-Jong Jeong^{1*}, Manoj Joshi², Timothy J. Osborn², Chang-Hoi Ho³, Shilong Piao^{4,5,6}, Deliang Chen⁷, Junguo Liu¹, Hong Yang^{8,9}, Hoonyoung Park³, Baek-Min Kim¹⁰, Song Feng¹¹

¹School of Environmental Science and Engineering, Southern University of Science and Technology (SUSTech), Shenzhen, China

²Climatic Research Unit, School of Environmental Sciences, University of East Anglia, Norwich, NR4 7TJ, UK

³School of Earth and Environmental Sciences, Seoul National University, Seoul, Republic of Korea

⁴Key Laboratory of Alpine Ecology and Biodiversity, Institute of Tibetan Plateau Research, Chinese Academy of Sciences, Beijing, China

⁵Sino-French Institute for Earth System Science, College of Urban and Environmental Sciences, Peking University, Beijing 100871, China

⁶Center for Excellence in Tibetan Earth Science, Chinese Academy of Sciences, Beijing 100085, China

⁷Department of Earth Sciences, University of Gothenburg, Gothenburg, Sweden

⁸EAWAG, Swiss Federal Institute of Aquatic Science and Technology, Dübendorf, Switzerland

⁹Faculty of Sciences, University of Basel, Basel, Switzerland

¹⁰Korea Polar Research Institution, Incheon, Korea

¹¹Department of Geosciences, University of Arkansas, Fayetteville, 72701, AR, USA

Nature Climate Change (Accepted)

*Corresponding author:

Prof. Su-Jong Jeong, School of Environmental Science and Engineering, South University of Science and Technology of China, Shenzhen 518055, Guangdong, China (sujong@sustc.edu.cn)

Aridity – the ratio of atmospheric water supply (precipitation; P) to demand (potential evapotranspiration; PET) – is projected to decrease (i.e., become drier) as a consequence of anthropogenic climate change, aggravating land degradation and desertification¹⁻⁶. However, the timing of significant aridification relative to natural variability – defined here as the time of emergence for aridification (ToEA) – is unknown, despite its importance in designing and implementing mitigation policy⁷⁻¹⁰. Here we estimate ToEA from projections of 27 global climate models (GCMs) under Representative Concentration Pathways (RCPs) RCP4.5 and RCP8.5, and in doing so, identify where emergence occurs before global mean warming reaches 1.5°C and 2°C above the pre-industrial level. Based on the ensemble median ToEA for each grid cell, aridification emerges over 32% (RCP4.5) and 24% (RCP8.5) of the total land surface before the ensemble median of global mean temperature change reaches 2°C in each scenario. Moreover, ToEA is avoided in about two-thirds of the above regions if the maximum global warming level is limited to 1.5°C. Early action for accomplishing the 1.5°C temperature goal can therefore dramatically reduce the likelihood of large regions facing significant aridification and related potential impacts.

Climate aridity is a useful concept for determining the background dryness or wetness of the land surface for given climate conditions, and is usually defined by the aridity index (AI), defined as a ratio of P to PET (P/PET)²⁻⁶. If the AI is less than 0.65, a region is classified as 'drylands'^{3,11}. Decreases in AI over large regions are an indication that the climate is getting drier, i.e., undergoing aridification: the expansion of the world's dryland area then increases the risks of land degradation, desertification²⁻⁴, and decreases terrestrial carbon sequestration². Substantial aridification is a serious threat to society because drier conditions due to aridification are favourable to drought and wildfire occurrence, which critically affect agriculture, water quality, vegetation productivity, forest mortality, and biodiversity¹²⁻¹⁶. In addition, projected aridification-prone areas overlap with regions at risk of severe drought, significant soil moisture depletion, and shifts in potential vegetation distributions¹⁷⁻¹⁹. Indeed, evidence exists suggesting that disparate impacts related to aridification are already underway. Drought severity has increased over the Mediterranean, southern Africa, and the eastern coast of Australia over the course of the 20th century¹⁸. Semiarid areas of Mexico, Brazil, southern Africa, and Australia have encountered desertification for some time²⁰. Over the Iberian Peninsula, increasing water demand has reduced the streamflow in rivers²¹.

Quantitative assessments of aridification related to future warming are therefore necessary to understand its potential impacts on human society. However, aridification under future climate scenarios is usually described using spatial differences in AI between specific periods of the 20th and 21st centuries (e.g., 2071-2100 minus 1961-1990)^{2,3}. Such an approach hides temporal aspects such as the time when the degree of aridification reaches a substantial level, which is important for climate adaptation^{22,23}. In this study we describe a time of emergence (ToE) for significant aridification. The ToE approach is widely used to examine the time that a climate signal (S) emerges from natural climate variability or noise (N)⁷⁻¹⁰.

We use climate projections for the historical period for 1861-2005 and the RCP4.5 and RCP8.5 scenarios for 2006-2100 from 27 GCMs that participated in CMIP5²⁴ (Table S1). The first ensemble member of each GCM is used and is adjusted to the observations based on bias-correction (see Supplementary information and Figs. S1, S2). ToEA is determined for each ensemble as a time when a signal-to-noise ratio (S/N) of annual mean AI exceeds a particular threshold (see examples in Fig. S3)⁸⁻¹⁰. The signal (S) is the decrease in AI driven by anthropogenic climate change under each RCP scenario, computed as the difference between each 20-year running average of annual-mean AI (from 1987-2006 to 2081-2100) and annual-mean AI for the present climate (1986-2005) (Fig. S4). Each 20-year running mean is indexed to its final year, thus, the ToEA range is 2006-2100. The noise (N) is computed as a standard deviation of annual mean AI for 1861-1910, when anthropogenic forcing was much smaller than during the present (Fig. S4)¹⁰. The 50-year period is long enough to include both interannual and interdecadal timescales of natural variability in our estimate of N¹⁰. The median, 84th and 16th percentile years, and the 16-84% range, of ToEA are calculated using the whole ensemble of model years across the 27 GCMs (see Methods and Fig. S5).

The S/N ratio threshold is set to 0.5, thus the ToEA is selected as the earliest year when there is a decrease in the 20-year mean AI that exceeds half the interannual standard deviation (i.e., $S/N < -0.5$). Any such threshold is somewhat subjective, but -0.5 is chosen as a result of both statistical and physical considerations: S/N should be large enough to represent a change with important practical implications, while not so large that it is equivalent to events that have little chance of occurring during the timescale of interest. Accordingly our threshold choice is based more on impacts rather than a confidence interval, as has been done previously⁹. Choosing S/N to be 0.5 with respect to the late 20th century period means that the probability of the occurrence of an annual AI anomaly in the 10th percentile, i.e. an AI

anomaly that occurs once per decade during the late 20th century is doubled (Fig. S6). A climate with an aridity change of -0.5 N can also be considered as a shift to continuous moderate drought conditions, on top of which interannual variability can cause episodic severe droughts²⁵.

Additionally, when evaluating the implications of global temperature targets, we should be aware that global temperature might overshoot such targets for 1-2 decades even with decreasing forcing because of the inertia of the climate system. A choice of $S/N < -0.5$ is small enough that anomalous years having an AI lower than 20th century AI minus 0.5 N are actually likely to be experienced in an overshoot regime lasting for only a few decades, which is necessary for planning practical adaptation strategies.

Figure 1 displays a physical and climatological rationale for choosing $S/N < -0.5$ by showing regions where the actual aridity classification would change if AI decreased everywhere by 0.5 N. Many regions along the boundaries of existing climatic regimes, such as the Sahel region in Africa, or the highly populated northern Indian subcontinent, would find themselves in different aridity regimes, implying profound climatic impacts. Globally, 9% of humid regions would become dry sub-humid, 6% of humid and dry sub-humid regions would become semi-arid, 15% of semi-arid regions would become arid, and 15% of arid regions would become hyper-arid. Such profound changes imply important effects on desertification, drought occurrence, and water management²⁻⁶.

Climate adaptation and mitigation policies are planned by policymakers according to the temperature goals of the Paris Agreement, which are 1.5°C and 2°C above the pre-industrial level²⁶. Determining whether a ToEA is arrived at earlier than global temperature changes of 1.5°C and 2°C warming target ($t_{1.5}$ and t_2) can verify the effectiveness of such temperature goals on preventing emerging aridification, as well as providing vital information on regional

climate mitigation. Here, $t_{1.5}$ and t_2 are computed as the times at which global temperatures reach 0.9°C and 1.4°C above 1986-2005, respectively, since the latter period was likely at least 0.6°C warmer than the pre-industrial level^{26,27}. Note that the median and 16-84% range of global warming across 27 GCMs ensemble is 0.6°C and $0.4\text{-}0.9^\circ\text{C}$ above the pre-industrial level for the period 1986-2005.

The median and 16-84% range of ToEA calculated from the 27-member CMIP5 ensemble is shown in Fig. 2. The 16-84% range of ToEA is given for regions where the 84th percentile year of ToEA is no later than 2100. Significant aridification ($S/N < -0.5$) occurs over 42% and 49% of the total land surface under the RCP4.5 and RCP8.5 scenarios respectively by 2100 (Figs. 2a, 2b). In general, spatial patterns of median ToEA are similar under the two RCP scenarios: relatively earlier ToEA (< 2050) occurs over most of South America, Central America, southern Europe, western and southern Africa, coastal Australia, and southern China, whereas over North America and northern Europe, ToEA is generally later than 2050. The 16-84% range of ToEA is computed in areas with earlier ToEA, indicating that earlier ToEA is connected to smaller uncertainty, as well as substantial aridification being very likely during the 21st century in these regions (Figs. 2c, 2d). The median year of ToEA is generally earlier in RCP8.5 than RCP4.5, indicating that very high emissions of greenhouse gases increase the likelihood of substantial aridification by the end of the 21st century.

The median year of ToEA is now compared to that of $t_{1.5}$ and t_2 : we use the notation “ $<$ ” to mean “earlier than”. $\text{ToEA} \leq t_{1.5}$ and $t_{1.5} < \text{ToEA} \leq t_2$ are shown for RCP 4.5 (Fig. 3a) and RCP8.5 (Fig. 3b). A particular point being located in a region with $\text{ToEA} \leq t_{1.5}$ indicates a 50% likelihood (based on the CMIP5 ensemble spread) that aridification emerges before a 1.5°C global temperature change is reached. Aridification emerges before 1.5°C in most of southern Europe (SEU). Areas with $\text{ToEA} \leq t_{1.5}$ are much smaller than those with $\text{ToEA} \leq t_2$ in five regions: Central America (CAM), South America (SAM) (in RCP 4.5 only), southern Africa

(SAF), coastal Australia (AUS), and southern China (SCH), indicating that in these regions limiting global warming to 1.5°C significantly reduces the likelihood of emerging aridification (see also Fig. S7), consistent with previous research about dryland expansion^{3,4,16}. In order to better investigate the uncertainties in ToEA in those regions where ToEA occurs before $t_{1.5}$ and t_2 , they are examined in more detail. An earlier ToEA might be expected due to both decreasing P and increasing PET (CAM, SAM, SEU, SAF, and AUS) or a larger increase in PET than P (SCH) (Fig. S8) which is driven by differing amounts of regional temperature change (Fig. S9).

Among the six regions, SEU has the earliest ToEA: indeed the 84th percentile year of ToEA is earlier than the median year of t_2 (stippled areas in Figs. 3a, 3b) under both RCP scenarios, indicating that many areas of SEU are very likely to undergo substantial aridification without significant climate mitigation. For the other five regions, the ranges of ToEA are mostly later than $t_{1.5}$, but earlier than t_2 under RCP 4.5 (Fig. 3c), while being certainly later than $t_{1.5}$, but not significantly earlier than t_2 under RCP 8.5 (Fig. 3d), suggesting that aridification depends not just on the final global temperature change that is encountered, but also on the emissions trajectory.

The areas in which aridity emerges before $t_{1.5}$ or t_2 are somewhat larger under RCP4.5 than under RCP8.5 in some regions such as CAM, SAF, and AUS despite the median GCM $t_{1.5}$ occurring half a decade or so later under RCP4.5 than under RCP8.5. For $ToEA \leq t_{1.5}$, this is because the lower (early aridification) part of the ToEA distribution (across GCMs and grid cells in each region) occurs at a similar time under the two scenarios despite the slightly later $t_{1.5}$ under RCP4.5 (Figs. 3c, 3d). We suggest that these differences are because of a nonlinear response of the hydrological cycle per degree of warming as global warming stabilises in some GCMs, causing enhanced warming and aridification in some locations relative to the mean warming²⁸. Differences in regional aerosol forcings between RCP4.5 and RCP8.5

might play some role, though previous work has found little effect on aridity averaged over global land in one GCM⁵.

The socio-economic impact of climate change depends on how much and how fast the changes happen as well as how many people are affected¹⁷. Fig. 4 shows the area and present-day population count over regions with $ToEA \leq t_{1.5}$ and $ToEA \leq t_2$, and their relative fractions of the total land area and population, under both RCP scenarios. Under the RCP4.5 and RCP8.5 scenarios, regions with median $ToEA \leq t_2$ account for 32% and 24% of total land surface, and 24% and 18% of the world's present population. However, regions with median $ToEA \leq t_{1.5}$ account for less than 10% of both area and population. The difference is quite stark, and suggests that approximately 20% of land area and 10% of people can avoid experiencing significant aridification if temperature rise is kept to 1.5°C rather than 2°C above pre-industrial levels.

The estimates of ToEA in this study might be sensitive to a number of factors; for instance, projected PET increases in a warmer climate are magnified by assuming a constant stomatal conductance of plants in GCMs²⁹, causing more aridification. Vegetation growth and plant cover feedbacks associated with climate change might also change the time at which significant aridity changes emerge in different parts of the world.

In this study we have shown that significant AI signals are projected to emerge during this century in sizable fractions of the world measured by both population and area. Keeping global warming to below 1.5°C above pre-industrial levels can reduce the likelihood of such emergent aridification in many regions compared to even a warming of 2°C. Because present mitigation policies do not appear to be sufficient to achieve the 1.5°C temperature goal³⁰, more efforts to mitigate global warming are therefore urgently needed to reduce the spread of

aridification, as well as aridity-related impacts and risks in many highly populated areas and regions of ecological significance around the world.

Figure Captions

Figure 1. Spatial distributions of AI and related climate regime in present climate, and regime changes if AI decreases by 0.5N. **a**, The spatial distribution of ensemble mean AI and 5 climate regimes based on AI in present climate^{3,11}. Gray areas indicate the Arctic circle (> 65°N). **b**, Changes in arid-type regimes when AI decreases by an amount of the half of its noise. White areas indicate regions with no regime change.

Figure 2. Spatial distributions of multi-model ensemble median year of ToEA and the 16-84% range. The median year of ToEA projected by 27 model projections under **a**, RCP4.5 and **b**, RCP8.5. Land areas where median ToEA does not occur by 2100 are left white. The 16-84% range (years) estimated under **c**, RCP4.5 and **d**, RCP8.5; white areas are where the 84th percentile year of ToEA occurs after 2100.

Figure 3. Spatial distributions of regions with $ToEA \leq t_{1.5}$ and $t_{1.5} < ToEA \leq t_2$, and proportions of GCM simulations that show $t_{1.5}$, t_2 , and ToEA in each particular year. **a,b**, Spatial maps of $ToEA \leq t_{1.5}$ (red) and $t_{1.5} < ToEA \leq t_2$ (light-blue) under (a) RCP4.5 and (b) RCP8.5. Those regions are determined by comparing the median of ToEA to that of $t_{1.5}$ and $t_{2.0}$, respectively. Six squares represent Central and South America (CAM and SAM), Southern Europe (SEU), southern Africa (SAF), coastal Australia (AUS), and south China (SCH), respectively. Stipples indicate that the 84th percentile year of ToEA is earlier than the median year of t_2 . **c,d**, Proportions of GCM simulations under (c) RCP4.5 and (d) RCP8.5. For $t_{1.5}$ and t_2 , proportions are computed based on the global mean temperature change. In each regions, ToEA values at all grid cells over the land surface are used to compute proportions. The black dots indicate the median of $t_{1.5}$, t_2 , and ToEA of six regions. White color indicates that less than 10% of models show $t_{1.5}$, t_2 , and ToEA at a particular year.

Figure 4. Total area and present-day population count over regions with $ToEA \leq t_{1.5}$ and $ToEA \leq t_2$ under the RCP4.5 and RCP8.5 scenarios. a, area, b, present-day population count. Light red and light blue colors denote regions where the median year of ToEA is earlier than that of $t_{1.5}$ and t_2 , respectively. Blue colors denote areas where the 84 percentile of the CMIP5 ensemble of years of ToEA is earlier than the median year of t_2 . The area where the 84 percentile year is earlier than the median year of $t_{1.5}$ is negligible ($< 0.15\%$).

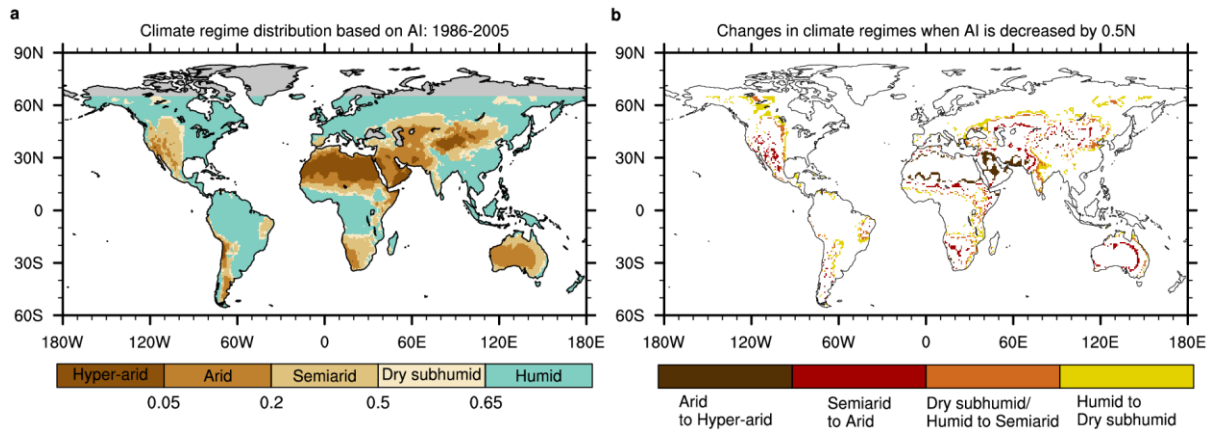


Figure 1.

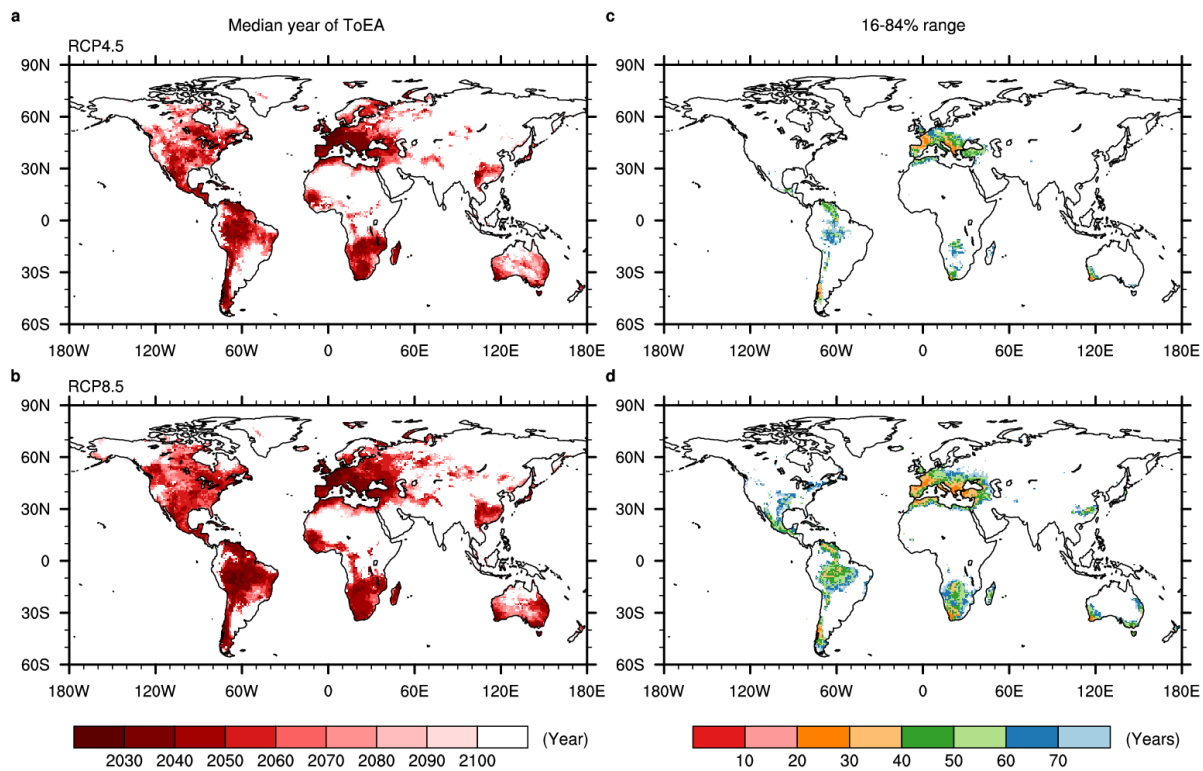


Figure 2.

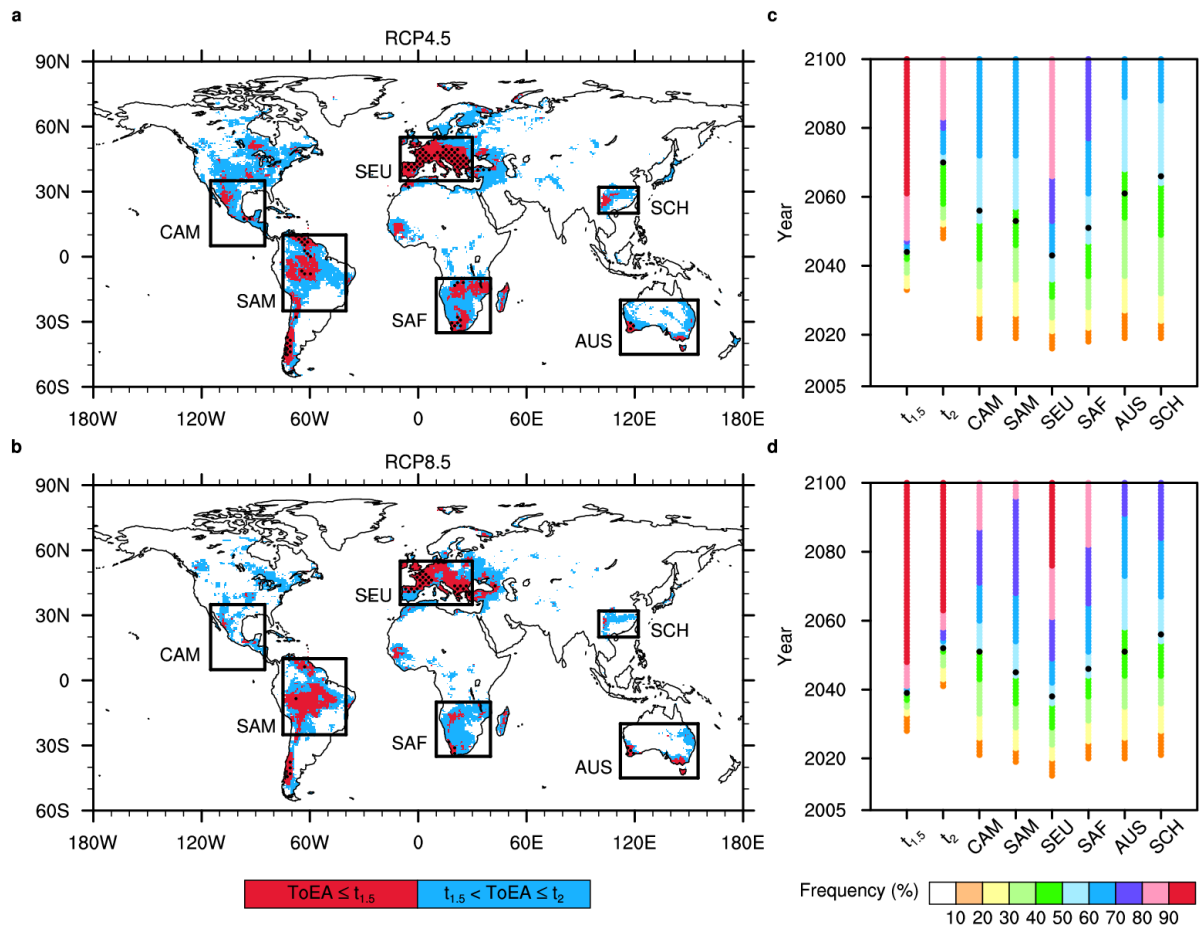


Figure 3.

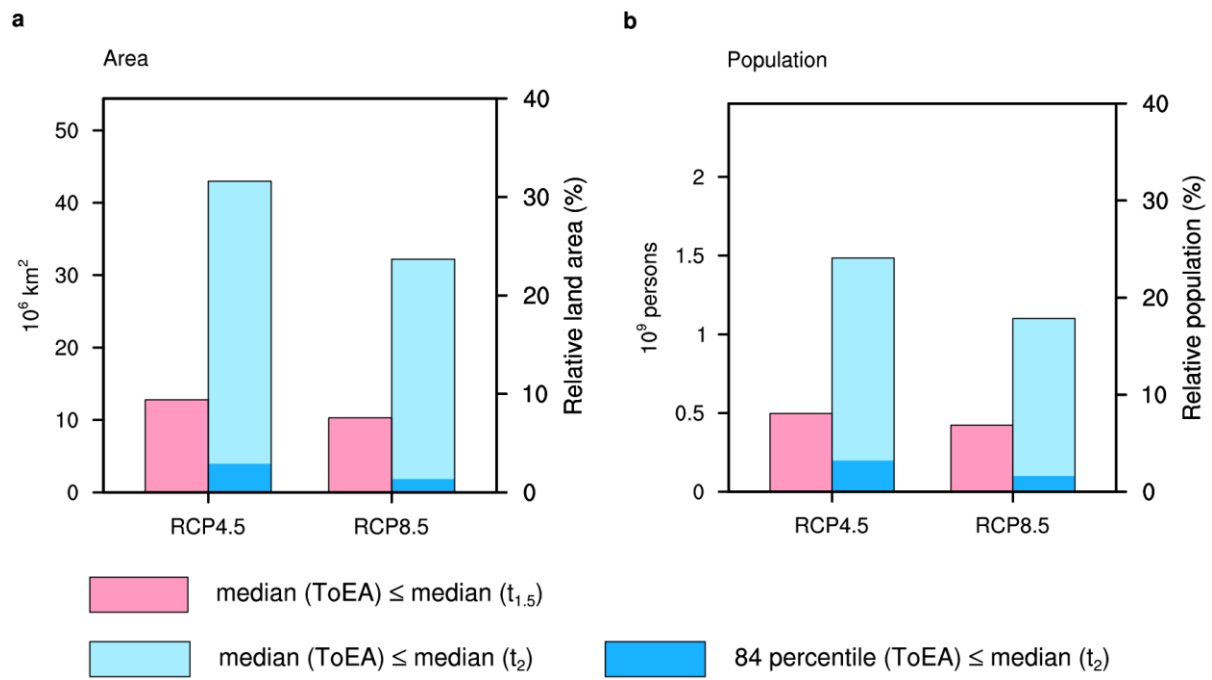


Figure 4.

Acknowledgements

Su-Jong Jeong and Chang-Eui Park were supported by the startup funding of the South University of Science and Technology of China. Junguo Liu was supported by the National Science Fund for Distinguished Youth Scholars (41625001). The part of research funding was provided by the Southern University of Science and Technology (Grant no. G01296001). Tim Osborn was supported by the Belmont Forum/JPI-Climate project INTEGRATE (NE/P006809/1). Manoj Joshi was supported by the UK Natural Environment Research Council Grant Robust Spatial Projections (NE/N018397/1). Chang-Hoi Ho and Hoonyoung Park were funded by the Korea Ministry of Environment as part of the “Climate Change Correspondence Program”. Baek-Min Kim was supported by Korea Polar Research Institute Project (PE17130).

Author contributions

C-EP and S-JJ conceived and designed the study, analysed data, and wrote the paper. MJ and TJO improved the study, provided data, and wrote the paper. C-HH, SP, DC, JL, HY, HP, B-MK wrote the paper. SF provided data and wrote the paper.

Competing financial interests

The authors declare no competing financial interests.

References

1. Collins, M. *et al.* Long-term Climate Change: Projections, Commitments and Irreversibility. *In Climate Change 2013: The Physical Science Basis*. Contribution of Working Group I to the Fifth Assessment Report of the Intergovernmental Panel on Climate Change [Stocker, T. F. *et al.* (eds.)]. Cambridge University Press, Cambridge, United Kingdom and New York, NY, USA (2013).
2. Huang, J., Yu, H., Guan, X., Wang, G. & Guo, R. Accelerated dryland expansion under climate change. *Nature Clim. Change* **6**, 166-171 (2016).
3. Feng, S. & Fu, Q. Expansion of global drylands under a warming climate. *Atmos. Chem. Phys.* **13**, 10081-10094 (2013).
4. Sherwood, S. & Fu, Q. A drier future? *Science* **343**, 737–739 (2014).
5. Lin, L., Gettelman, A., Fu, Q. & Xu, Y. Simulated differences in 21st century aridity due to different scenarios of greenhouse gases and aerosols. *Climatic Change Online* doi:10.1007/s10584-016-1615-3 (2016).
6. Fu, Q., Lin, L., Huang, J., Feng, S. & Gettelman, A. Changes in terrestrial aridity for the period 850-2080 from the Community Earth System Model. *J. Geophys. Res. Atmos.* **121**, doi :10.1002/2015JD024075 (2016).
7. Mahlstein, I., Knutti, R., Solomon, S. & Portmann, R. W. Early onset of significant local warming in low latitude countries. *Environ. Res. Lett.* **6**, 034009 (2011).
8. Hawkins, Ed. & Sutton, R. The potential to narrow uncertainty in projections of regional precipitation change. *Clim. Dyn.* **37**, 407-418 (2011).
9. Hawkins, Ed. & Sutton, R. Time of emergence of climate signals. *Geophys. Res. Lett.* **39**, L01702 (2012).
10. King, A. D. *et al.* The timing of anthropogenic emergence in simulated climate extremes.

- Environ. Res. Lett.* **10**, 094015 (2015).
11. Middleton, N. *et al.* *World atlas of desertification 2nd edn* (Arnold, Hodder Headline, PLC, 1997).
 12. Mosley, L. M. Drought impacts on the water quality of freshwater systems; review and integration. *Earth-Science Reviews* **140**, 203-214 (2015).
 13. Westerling, A. L., Hidalgo, H. G., Cayan, D. R. & Swetnam, T. W. Warming and Earlier Spring Increase Western U.S. Forest Wildfire Activity. *Science* **313**, 940-943 (2006).
 14. Novick *et al.* The increasing importance of atmospheric demand for ecosystem water and carbon fluxes, *Nature Clim. Change* **6**, 1023-1027 (2016).
 15. Webber *et al.* Uncertainty in future irrigation water demand and risk of crop failure for maize in Europe, *Environ. Res. Lett.* **11**, 074007 (2016).
 16. Huang, J. Yu, H. Dai, A. Wei Y. & Kang, L. Drylands face potential threat under 2 °C global warming target, *Nature Clim. Change* **7**, 417-422 (2017).
 17. Sedláček, J., Knutti, R. Half of the world's population experience robust changes in the water cycle for a 2 °C warmer world. *Environ. Res. Lett.* **9**, 044008 (2014).
 18. Dai, A. Increasing drought under global warming in observations and models. *Nature Clim. Change* **1**, 52-58 (2012).
 19. Gonzalez, P., Neilson, R. P., Lenihan, J. M. & Drapek, R. J. Global patterns in the vulnerability of ecosystems to vegetation shifts due to climate change. *Global Ecol. Biogeogr.* **19**, 755-768 (2010).
 20. D'Odorico, P., Bhattachan, A., Davis, K. F., Ravi, S. & Runyan, C. W. Global desertification: Drivers and feedbacks. *Advances in Water Resources* **51**, 326-244 (2013)
 21. Vicente-Serrano, S. M. *et al.* Evidence of increasing drought severity caused by temperature rise in southern Europe. *Environ. Res. Lett.* **9**, 044001 (2014).

22. Joshi, M., Hawkins, Ed., Sutton, R., Lowe, J. & Frame, D. Projections of when temperature change will exceed 2 °C above pre-industrial levels, *Nature Clim. Change* **1**, 407-412 (2011).
23. Park, C.-E., Jeong, S.-J., Ho, C.-H. & Kim, J. Regional Variations in Potential Plant Habitat Changes in Response to Multiple Global Warming Scenarios, *J. Clim.* **28**, 2884-2899 (2015).
24. Taylor, K. E., Stouffer, R. J. & Meehl, G. A. An Overview of CMIP5 and the Experiment Design. *Bull. Amer. Meteor. Soc.* **93**, 485-498 (2011).
25. Barbeta, A. *et al.* The combined effects of a long-term experimental drought and an extreme drought on the use of plant-water sources in a Mediterranean forest. *Glob. Change Biol.* **21**, 1213-1225 (2015).
26. Schleussner, C.-F. *et al.* Science and policy characteristics of the Paris Agreement temperature goal. *Nature Clim. Change*, **6**, 827-835 (2016).
27. Hawkins, Ed. *et al.* Estimating changes in global temperature since the pre-industrial period. *Bull. Amer. Meteor. Soc.* **Online** doi:10.1175/BAMS-D-16-0007.1 (2017).
28. Caesar, J. *et al.* Response of the HadGEM2 Earth System Model to Future Greenhouse Gas Emissions Pathways to the Year 2300. *J. Clim.* **26**, 3275-3284 doi:10.1175/JCLI-D-12-00577.1 (2012).
29. Milly, P. C. D. & Dunne, K. A. Potential evapotranspiration and continental drying. *Nature Clim. Change* **6**, 946-949 (2016).
30. Rogelj, J. *et al.* Paris Agreement climate proposals need a boost to keep warming well below 2 °C. *Nature* **534**, 631-639 (2016).

Methods

Climate projection dataset

Five monthly variables from 27 global climate models (GCMs; Table S1) are selected for our analysis: precipitation (P), surface air temperature (TAS), surface downwelling solar radiation, specific humidity, and wind speed. The time of global warming target, $t_{1.5}$ and t_2 , is computed based on the direct model output TAS, whereas the model output was regridded and bias-corrected prior to the calculation of PET and aridity index (AI). The variables over the land surface were interpolated to $0.5^\circ \times 0.5^\circ$ in latitude and longitude and then bias-corrected using gridded observation data from the Climate Prediction Center^{31,32} (CPC; see Ref. 3 for detail). Four variables (TAS, solar radiation, specific humidity and wind speed) were used to compute PET based on the Penman-Monteith method^{3,33}. All subsequent analyses use 20-year equal-weight running mean P, PET, TAS, and AI, from 1986-2005 to 2081-2010, to remove interannual fluctuations. Each 20-year running average is indexed to its final year (e.g. 20-year running mean TAS for 2060 is an average of TAS for 2041-2060). In the case of 2020, the running average uses the historical simulation for the first five years (2001-2005) and each RCP scenario for the other 15 years (2006-2020).

Calculation of multi-model ensemble median, 84th and 16th percentile years of the ToEA

For all individual GCMs, ToEA is defined as a time when the signal-to-noise ratio (S/N) of AI is decreased below -0.5 firstly. Based on the ToEA from individual projections, the median, 84th and 16th percentile years of the ToEA are calculated (Fig. S5). We first classify the 27 models into three categories for each grid point: A, emergence of decreased AI ($S/N < -0.5$, i.e., ToEA); B, emergence of increased AI ($S/N > 0.5$); C, no emergence. The median, 84th and 16th percentile years of the ToEA are calculated only if the following two conditions are both satisfied: 1) the ToEA is estimated for 14 models ($> 50\%$ of 27 models) at least, 2) the

number of models showing emergence of increased AI is less than 9 (< 33% of 27 models). Note that the second condition is referring to the probability of the statement “unlikely”³⁴. The calculation of the median, 84th and 16th percentile years of the ToEA is done assuming that the ToEA of any models falling in subsets B and C is later than 2100. For example, if an arbitrary grid point has 24 models showing a ToEA and 3 models showing no emergence, we calculate the median, 84th and 16th percentile years of the ToEA using 27 models (with 3 set to >2100). For another grid point with 17 GCMs decreasing emergence, 6 increasing emergence, and 4 no emergence, both the median and 16th percentile years of the ToEA are computed, but the 84th percentile year is not. As another example, an arbitrary grid point with ToEA estimated for 15 models, whereas 10 models show the emergence of increased AI, we classify this point as “no consistency” and don’t compute any of the indicators. The 16-84% range of ToEA is computed as the difference between 84th and 16th percentile year of ToEA when the 84th percentile year of ToEA is no more than 2100.

Population count dataset

We used the gridded population count dataset from the Shared Socioeconomic Pathways (SSPs)³⁵ which have been downscaled from country level urban and nonurban population data to 0.5-degree grids. For the period 1980-2010, the country population comes from International Monetary Fund data (<http://www.imf.org/data>) and here we use population count of 2010, indicating a time-independent assumption in our analysis. In addition, we changed a quasi-regular grids given by the World Geodetic System WGC84 into a regular half-degree grids by matching the closest grid point between the original and regular grids.

Data availability

High-resolution gridded datasets from Climate Research Unit Times Series version 4

(CRUTS4) is available on data server of Centre for Environmental Data Analysis (CEDA) (http://data.ceda.ac.uk/badc/cru/data/cru_ts/cru_ts_4.0). The original CMIP5 data is available at the CMIP5 data portal (<https://esgf-node.llnl.gov/search/cmip5>). Annual mean aridity index based on CPC data and the bias-corrected CMIP5 data are available upon request to the corresponding author Su-Jong Jeong (waterbell77@gmail.com).

References

31. Chen, M. Xie, P. Janowiak, J. E. & Arkin, P. A. Global land precipitation: a 50-yr monthly analysis based on gauge observations, *J. Hydrometeorol.* **3**, 249-266 (2002).
32. Fan, Y. & van den Dool, H. A global monthly land surface air temperature analysis for 1948-present. *J. Geophys. Res.* **113**, D01103, doi:10.1029/2007JD008470 (2008).
33. Allen, R. G. Pereira, L. S., Raes, D. & Smith, M. Crop evapotranspiration—guidelines for computing crop water requirements—FAO Irrigation and drainage Paper 56. (*FAO, 1998*).
34. Mastrandrea, M. D. *et al.* Guidance Note for Lead Authors of the IPCC Fifth Assessment Report on Consistent Treatment of Uncertainties, *Intergovernmental Panel on Climate Change (IPCC)*, <http://www.ipcc.ch> (2010).
35. Murakami, D. & Yamagata, Y. Estimation of gridded population and GDP scenarios with spatially explicit statistical downscaling, *ArXiv*, **1610.09041**, [URL:https://arxiv.org/abs/1610.09041](https://arxiv.org/abs/1610.09041) (2016).